Electronic Supplementary Material (ESI) for Journal of Materials Chemistry A.

Supporting Information

Rh/RhO$_x$ nanosheets as pH-universal bifunctional catalysts for hydrazine oxidation and hydrogen evolution reactions

Junjun Yang[#,a], *Liang Xu*[#,a], *Wenxiang Zhu*[a], *Miao Xie*[a], *Fan Liao**[,a], *Tao Cheng**[,a], *Zhenhui Kang*[a,b], *Mingwang Shao**[,a]

[a]Institute of Functional Nano & Soft Materials (FUNSOM), Jiangsu Key Laboratory for Carbon-Based Functional Materials & Devices, Soochow University, Suzhou 215123, P. R. China
[b]Macau Institute of Materials Science and Engineering, Macau University of Science and Technology, Macau, China.

E-mail addresses: fliao@suda.edu.cn (F. Liao), tcheng@suda.edu.cn (T. Cheng), mwshao@suda.edu.cn (M. Shao)

1. Experiments

1.1. Materials

The $RhCl_3 \cdot 3H_2O$, commercial 20 wt% Rh/C and KOH were purchased from Aladdin Industrial Corporation. Potassium hydroxide and Nafion (5 wt %) was purchased from Sigma-Aldrich Co. The continuous ultrathin carbon layer on a holey carbon/formvar support film were purchased from Zhongjingkeyi(Beijing) Film Technology Co., LTD. The commercial 20 wt% Pt/C catalyst was from Alfa Aesar Co. Other reagents were analytical reagent grades without further purification. The water used throughout the experiment was double distilled water.

1.2. Synthesis of layered RhO_x nanosheets

The layered RhO_x nanosheets were fabricated as follows: Firstly, 50 mg $RhCl_3.3H_2O$ and 10 mL 6.0 M KOH solution were mixed and stirred to form a ginger yellow liquid. Then the solution was evaporated to dryness. The obtained powders were transferred to a crucible and calcined in a muffle furnace at 500 °C for 2 h with a heating rate of 10 °C min^{-1}. The obtained sample is denoted as RhO_x-500. In order to study the effect of calcination temperature on the nanostructure and catalytic activity, the calcinations were carried out at 300, 400 and 600 °C, with the samples named as RhO_x-300, RhO_x-400, RhO_x-600, while maintaining the invariance of other parameters and steps.

1.3. Synthesis of Rh/RhO_x nanosheets

The obtained RhO_x nanosheets were treated by Ar/H_2 (V : V = 95:5) gas purchased from Suzhou Jinhong Gas Co. The specific operation is to put the porcelain boat with 10 mg RhO_x nanosheets into the center of the tubular furnace and plug the foam plug at the furnace mouth. After vacuuming for 10 min, the Ar/H_2 (V : V = 95 : 5) gas was injected with a flow rate of 60 mL / min for 1 h at 200 °C. The treated samples are denoted as Rh/RhO_x-calcination temperature.

1.4. Materials characterizations

The scanning electron microscope image of the sample was obtained on a scanning electron microscope (Zies Supra 55) equipped with EDAX, which used Cu sheet as a substrate. XRD (Philips X'pert PRO MPD diffractometer) equipped with CuKα radiation ($\lambda = 0.15406$ nm), characterizing the phase and crystallography of all as-prepared samples. Transmission electron microscope (TEM) image, high-resolution TEM (HRTEM) image and elemental mapping were acquired by FEI Tecnai F20 transmission electron microscope with an accelerating voltage of 200 kV. The elements and chemical valence states of the sample were obtained from x-ray photoelectron spectroscopy (XPS) of Kratos AXIS UltraDLD ultra-high vacuum surface analysis system with Al Kα radiation (1486 eV) as a probe. The content of O and H were obtained from Organic Element Analyzer (EA) by Vario EL Cube.

1.5. Electrochemical Measurements

The electrochemical test was carried out with the CHI750 C electrochemical workstation using a typical three-electrode system. The glassy carbon electrode (GCE) with a diameter of 3 mm was used as the working electrode, a silver chloride electrode (Ag/AgCl), and a saturated calomel electrode (Hg/Hg_2Cl_2) as the reference electrode, and a carbon rot as the counter electrode.

The working electrode was prepared as follows: In order to improve the conductivity of Rh/RhO_x nanocomposites, carbon black ($m_{carbon\ black}$: m_{sample} = 4:1) was added in the electrochemical test of the catalyst. Then 2 mg catalyst was taken out to add in 900 μL 5:1 v/v of water isopropanol mixed solvent and 100 μL 0.5 wt% Nafion solution. The mixture was stirred with ultrasonic for 0.5 h. And 5 μL of the suspension was loaded onto the electrode (142 μg cm^{-2}). In this test, the hydrogen evolution was carried out in the oxygen-free 1.0 M KOH, 1.0 M PBS, and 0.5 M H_2SO_4 solution. Tests for HzOR were carried out in the oxygen-free 1.0 M KOH/0.5 M N_2H_4, 1.0 M PBS/0.3 M N_2H_4, 0.5 M H_2SO_4/0.5 M N_2H_4. All potentials in this study were converted to RHE reference scale according to the equation of E (vs.RHE) = E (vs.Ag/AgCl) + 0.197 V + pH*0.0591 V in the test of alkaline and neutral solution, E (vs.RHE) = E (vs.Hg/Hg_2Cl_2) + 0.245 V + pH*0.0591 V in acid solution test. All linear sweep voltammetry (LSV) curves are treated by 95% iR-corrected. 100 μL catalyst ink (2mg / mL) was dropped onto carbon paper (1 cm * 1 cm) before the stability test. The stability test was performed at the current density of 10 mA cm^{-2}. Electrochemical impedance spectroscopy (EIS) plots of all catalysts were tested at the frequency ranging from 100 kHz to 0.1 Hz. Faradaic efficiency (FE) of OHzS was determined by a gas chromatograph (GC Agilent 7890B). Rh/RhO_x-500 was tested at a current density of 10 mA cm^2 for 1 h, and the data were collected at an interval of 15 min.

1.6. Computational details

All calculations were carried out using the VASP software.[S1-S3] We used the Perdew, Burke, and Ernzerhof (PBE) flavor[S4] of DFT (Density of Functional Theory) with DFT-D_3 correction for London disperse (van der Waals attraction) with Becke-Johnson damping.[S5] The projector augmented wave (PAW) method was used to account for core-valence interactions.[S6] [S7] The kinetic energy cutoff for plane wave expansions was set to 400 eV, and reciprocal space was sampled by Γ-centered Monkhorst-Pack scheme with a grid of 3 * 3 * 1. The vacuum layer is at least 15 Å above the surface. The convergence criteria are 1 x 10^{-6} eV energy differences for solving the electronic wave function. All atomic coordinates were converged to within 1 x 10^{-2} eV/Å for maximal components of forces.

In this work, all free energies were calculated as

$$G_{298.15} = E_{elec} + E_{zpve} - T * S_m^v$$

The vibrational frequencies were evaluated for only surface adsorbate and were calculated. According to the calculated frequency results, we obtain the zero-point vibrational energy(zpve) and adsorption entropy S_m^v.

$$S_m^v = \sum_{\tilde{v}}^{\tilde{v}i} R\{\frac{\beta hc\tilde{v}}{e^{\beta hc\tilde{v}} - 1} - ln(1 - e^{-\beta hc\tilde{v}})\}$$

Where R is gas constant, β is 1/T*K_b (K_b is Boltzman constant), h is Plank constant, c is light speed, and v is wave number.

We carried out simulations for two systems, including Rh(111), Rh/RhO_x for HzOR (hydrazine reduction reaction), and for HER (Hydrogen Evolution Reaction). The simulated system also included Pt(111). The Pt(111) and Rh(111) surfaces were modeled by 3 * 3 unit cell with four periodic atom layers, and a vacuum thickness set (15 Å and 20 Å) separately were used to remove any interactions between slabs. For Rh/RhO_x structure, one Rh atom of the top layer of the Rh(111) system was replaced by O atoms forming Rh/RhO_x interface system, and two water molecules were placed on the surface to simulate HER. For Rh/RhO_x, Rh was replaced by O atom at the middle position of the boundary of two bottom layers on Rh(111), used for HzOR. During the geometry optimizations, the atoms in the bottom two layer were fixed, whereas the rest of the atoms were allowed to relax. The adsorption energies (E_{ads}) on the H atom for HER were calculated according to

$$\Delta G_{ads} = G_{*H} - G_{*} - \frac{1}{2} G_{H_2} \quad (1)$$

Where G_{*H} (* asterisk represents surface), G_*, and G_{H_2} represent the free energies of the corresponding intermediate (Pt(111), Rh(111) surface, or Rh/RhO_x), surface and H_2 in the gas phase, respectively.

The reaction energies for a series of intermediates on HzOR were calculated according to (2)-(9)

$$\Delta G_{ads;N_2H_4} = G_{*N_2H_4} - G_{N_2H_4} - G_{*} \quad (2)$$

$$\Delta G_{N_2H3} = G_{*N_2H3} + G_{\frac{1}{2}H_2} - G_{*N_2H_4} \quad (3)$$

$$\Delta G_{NNH_2} = G_{*NNH_2} + G_{\frac{1}{2}H_2} - G_{*N_2H_3} \quad (4)$$

$$\Delta G_{NHNH} = G_{*NHNH} + G_{\frac{1}{2}H_2} - G_{*N_2H_3} \quad (5)$$

$$\Delta G_{NNH} = G_{*NNH} + G_{\frac{1}{2}H_2} - G_{*NNH_2} \quad (6)$$

$$\Delta G_{NNH} = G_{*NNH} + G_{\frac{1}{2}H_2} - G_{*NHNH} \quad (7)$$

$$\Delta G_{N_2} = G_{*N_2} + G_{\frac{1}{2}H_2} - G_{*NNH} \quad (8)$$

$$\Delta G_{des;N_2} = G_{N_2} - G_{*} - G_{(N_2)} \quad (9)$$

Where $G_{*N_2H_4}$, $G_{*N_2H_3}$, G_{*NNH_2}, G_{*NHNH}, G_{*NNH}, G_{*N_2} represent the free energies of intermediates in elementary steps for HzOR. G_{*} represents the free energy of the surface (Rh(111), Rh/RhO$_x$). $G_{N_2H_4}$, $G_{\frac{1}{2}H_2}$, $G_{(N_2)}$ represent the free energies of molecule in the gas phase.

In the calculation of free energies, we have considered the top site, bridge site and two hollow sites (hpc and fcc) and structure. The lowest one was also reported in the manuscript on intermediates, reactants, and production. The calculated results show that the most stable site of H atom in all systems is the fcc site, the most stable sites of N_2H_4, NH_2NH, NHNH, NNH, N_2 are top site, bridge site, bridge site, bridge site, top site separately in Rh(111) system, the most stable sites of N_2H_4, $NHNH_2$, NNH_2, NNH, N_2 are top site, bridge site, hollow site, bridge site, the top site in Rh/RhO$_x$ system. We took structure into consideration, the free energy of vN_2 (v vertical) is lower than pN_2 (p paralleled), and other intermediates tend to parallel to the surface except for N_2 and *NH_2NH_2 in all systems, the free energy of NHNH is lower than in NNH_2 in Rh(111) system and reverse in Rh/RhO$_x$.

2. Supplementary figures

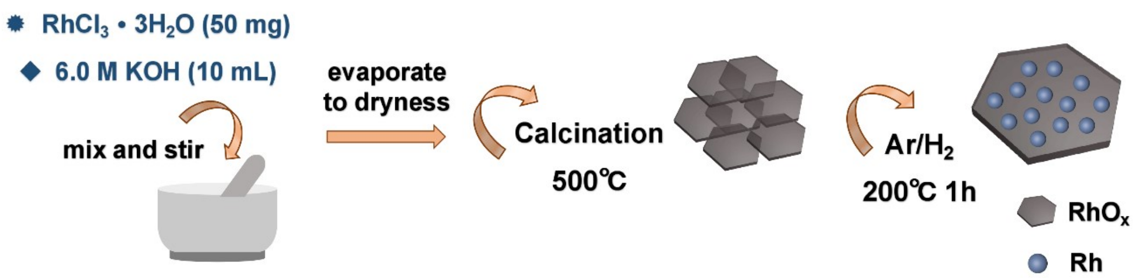

Figure S1. Schematic illustration of the formation process of Rh/RhO$_x$-500 electrode.

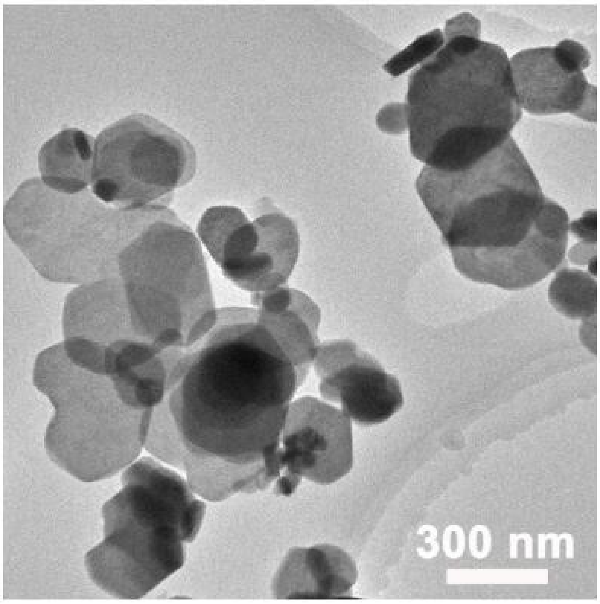

Figure S2. TEM image of RhO_x-500.

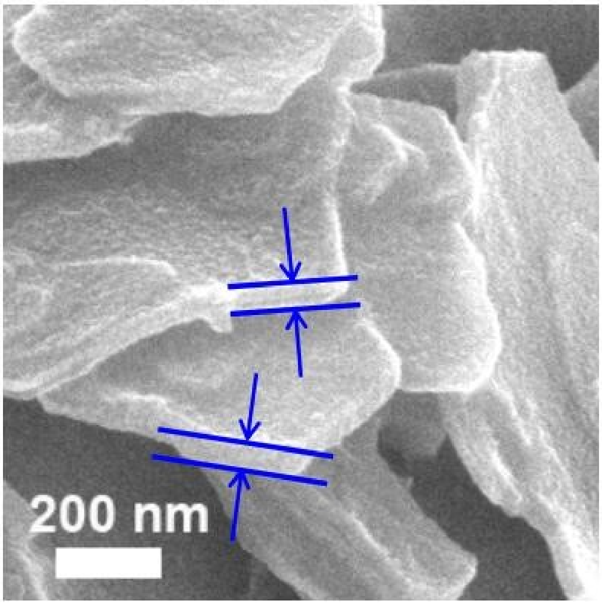

Figure S3. SEM image showing the side view for RhO_x-500.

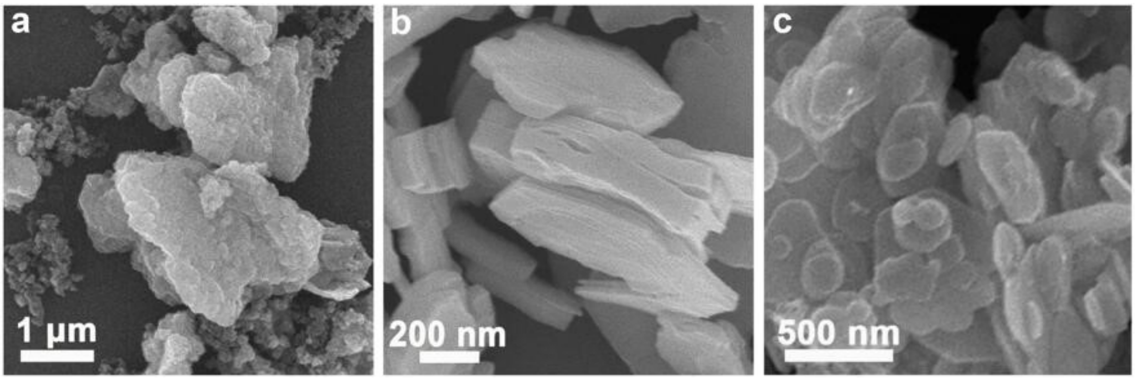

Figure S4. SEM images of RhO_x precursor with different calcination temperatures. (a) RhO_x-300; (b) RhO_x-400 and (c) RhO_x-600.

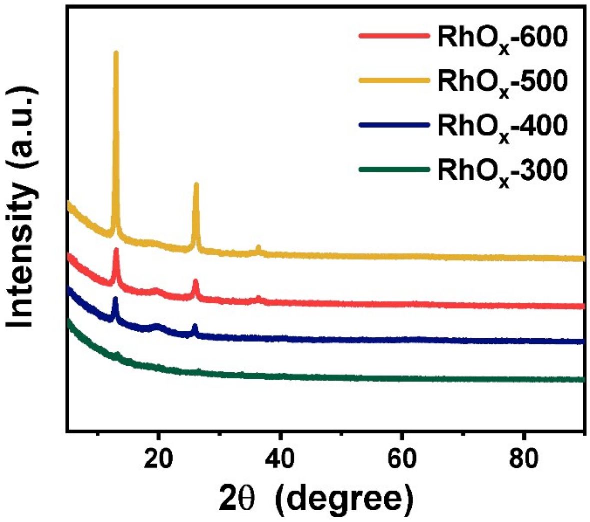

Figure S5. XRD patterns of RhO_x precursors with different calcination temperatures ranging from 300-600 °C.

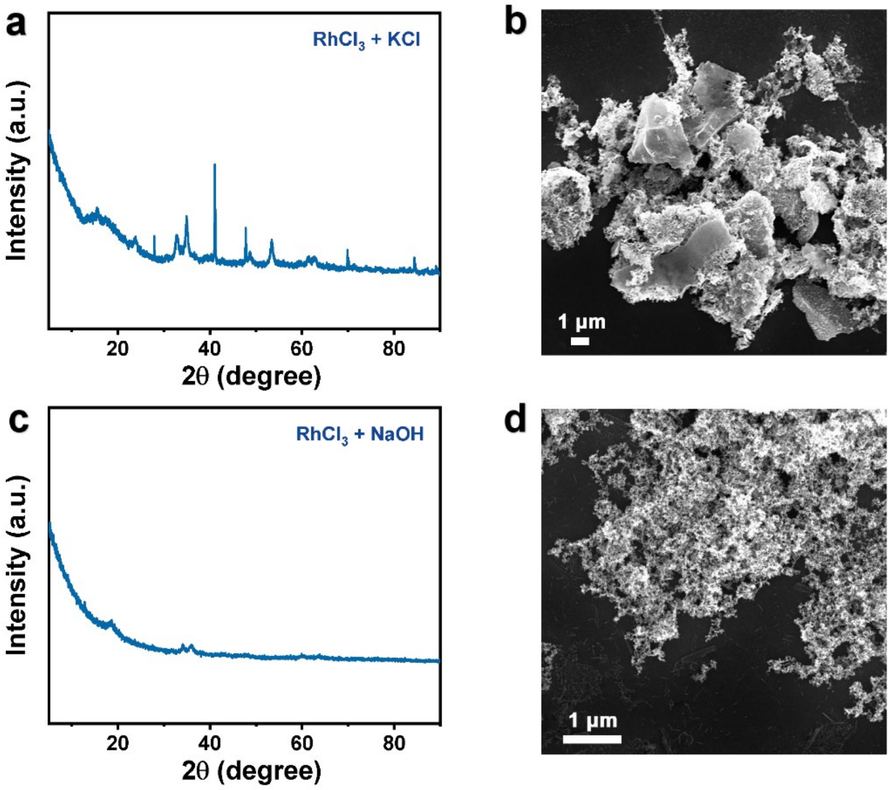

Figure S6. XRD patterns and SEM images of samples using different raw materials. (a) XRD pattern and (b) SEM image of products using KCl and $RhCl_3$ as raw materials. (c) XRD pattern and (d) SEM image of products using NaOH and $RhCl_3$ as raw materials.

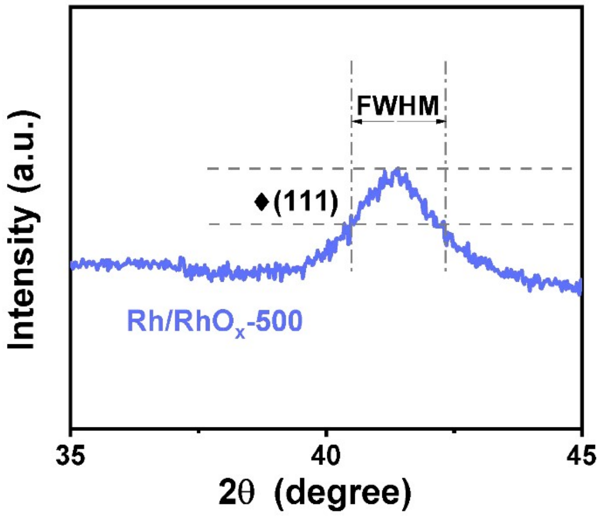

Figure S7. Calculation of Rh nanoparticle size by Scherrer formula. The expression of Scherrer's formula is D=Kλ/(βcosθ), where K is a constant (0.89), λ is the X-ray wavelength of 0.15406 nm, β is the full width at half maxima of the diffraction peak which converted to radian system (0.746), θ is the diffraction angle (41.4 °). D = 11.9 nm.

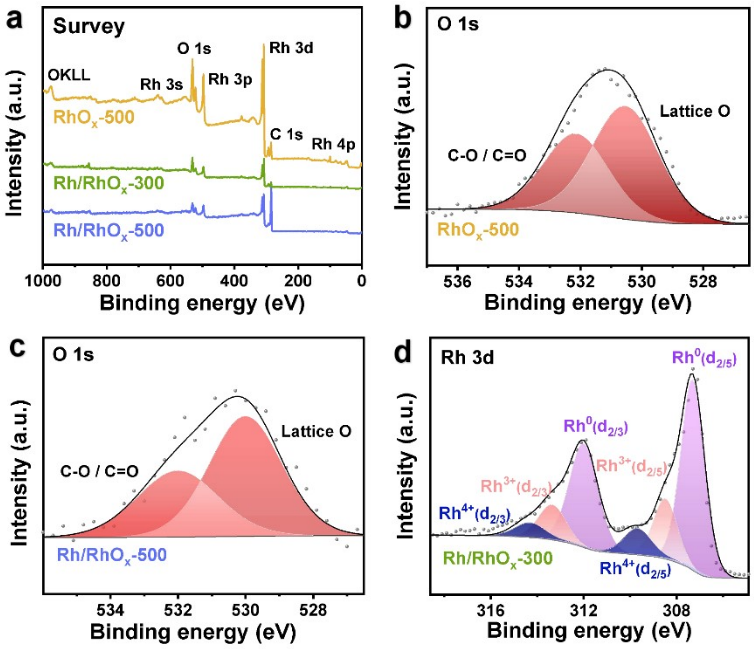

Figure S8. (a) Comparison of XPS survey spectra for RhO_x-500, Rh/RhO_x-300 and Rh/RhO_x-500. (b) XPS spectra of O 1s for RhO_x-500 and (c) Rh/RhO_x-500. (d) XPS spectrum of Rh 3d for Rh/RhO_x-300.

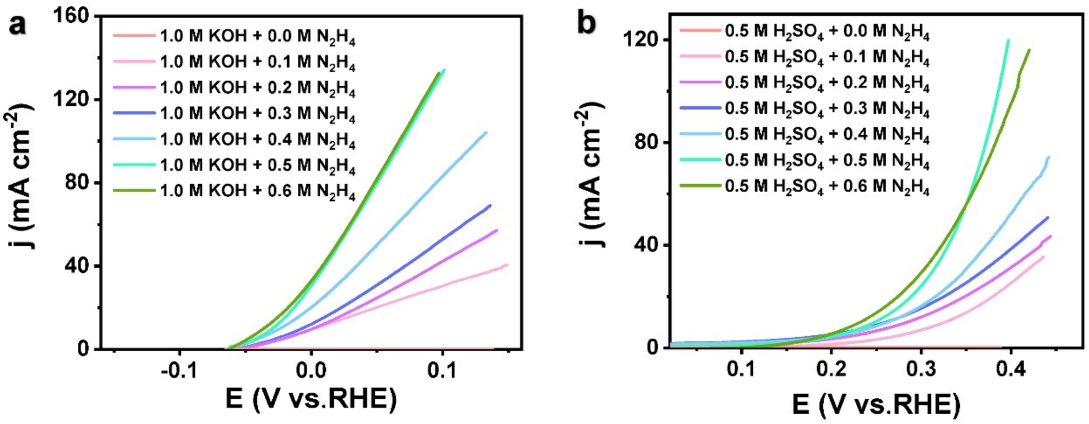

Figure S9. LSV curves of Rh/RhO_x-500 toward different concentrations of hydrazine in (a) 1.0 M KOH and (b) 0.5 M H_2SO_4.

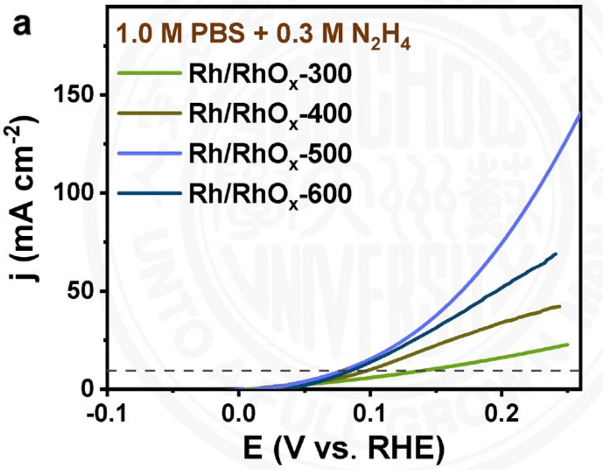

Figure S10. The LSV curves of RhO_x after calcinating at different temperatures for HzOR in 1.0 M PBS/0.3 M N_2H_4.

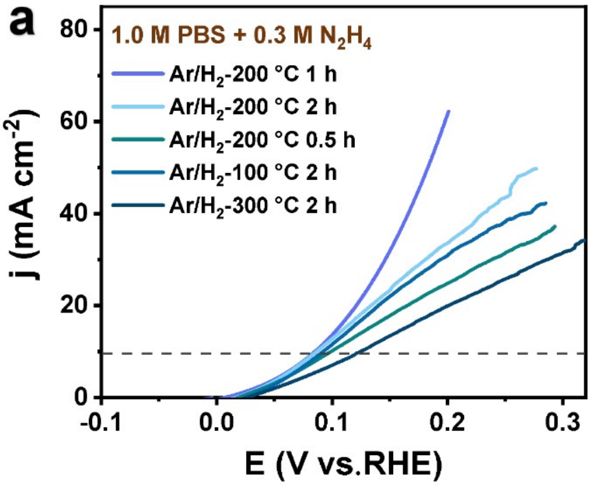

Figure S11. The LSV curves for HzOR of Rh/RhO$_x$-500 obtained by different treatment time and temperature of Ar/H$_2$.

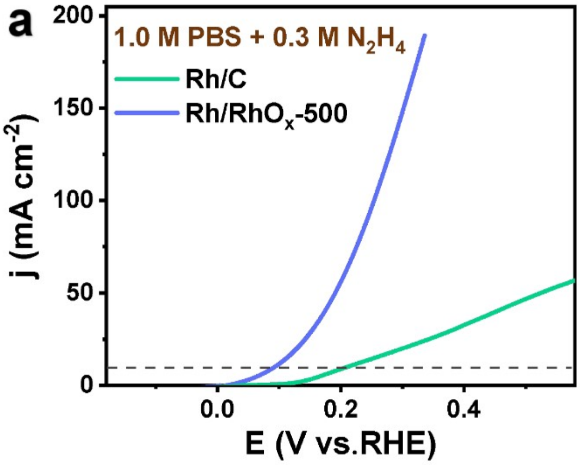

Figure S12. LSV curves of Rh/RhO$_x$-500 and Rh/C in 1.0 M PBS/0.3 M N$_2$H$_4$ for HzOR.

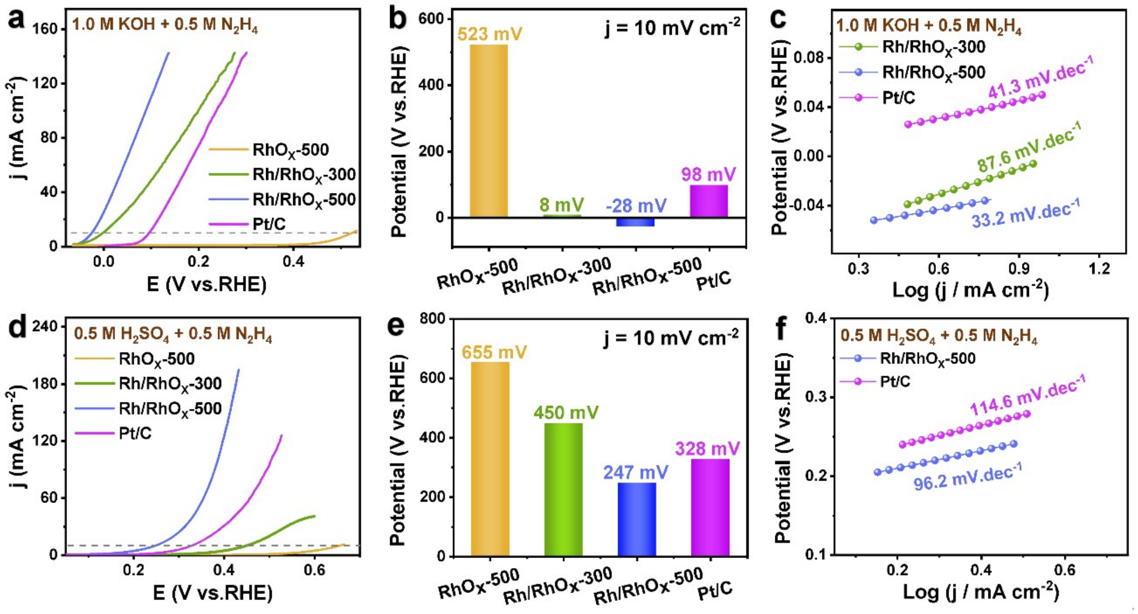

Figure S13. The electrocatalytic activity for HzOR in alkaline and acid medium. (a) The LSV curves of different catalysts and (b) corresponding potential (@10 mA cm^{-2}) comparison in 1.0 M KOH/0.5 M N_2H_4. (c) Tafel plots derived from (a). (d) The LSV curves of different catalysts and (e) corresponding potential (@10 mA cm^{-2}) comparison in 0.5 M H_2SO_4/0.5 M N_2H_4. (c) Tafel plots derived from (d).

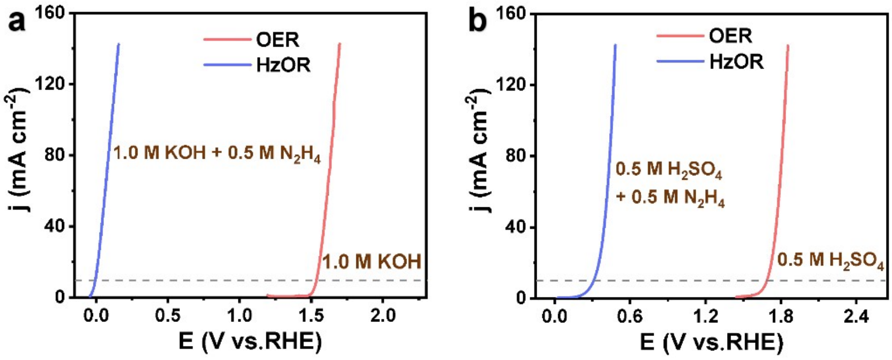

Figure S14. The LSV curves for OER and HzOR in alkaline and acidic electrolytes respectively.

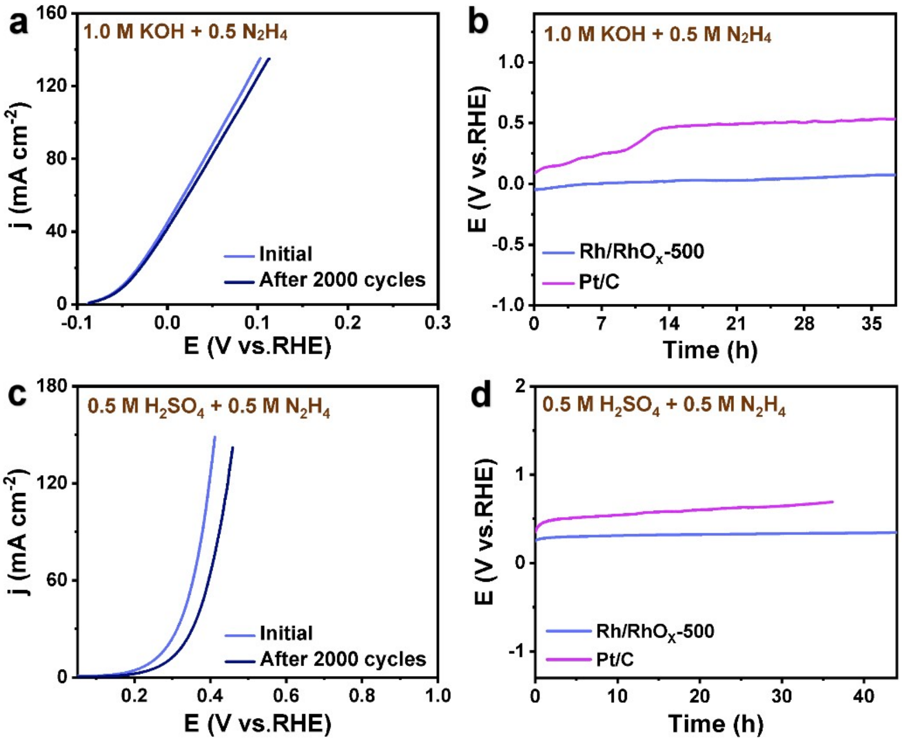

Figure S15. (a) The LSV curves of Rh/RhO$_x$-500 before and after 2000 CV circles and (b) the chronopotentiometric stability of Rh/RhO$_x$-500 recorded at 10 mA cm^{-2} current density in 1.0 M KOH/0.5 M N_2H_4. (c) The LSV curves of Rh/RhO$_x$-500 before and after 2000 CV circles and (d) the chronopotentiometric stability of Rh/RhO$_x$-500 recorded at 10 mA cm^{-2} current density in 0.5 M H_2SO_4/0.5 M N_2H_4.

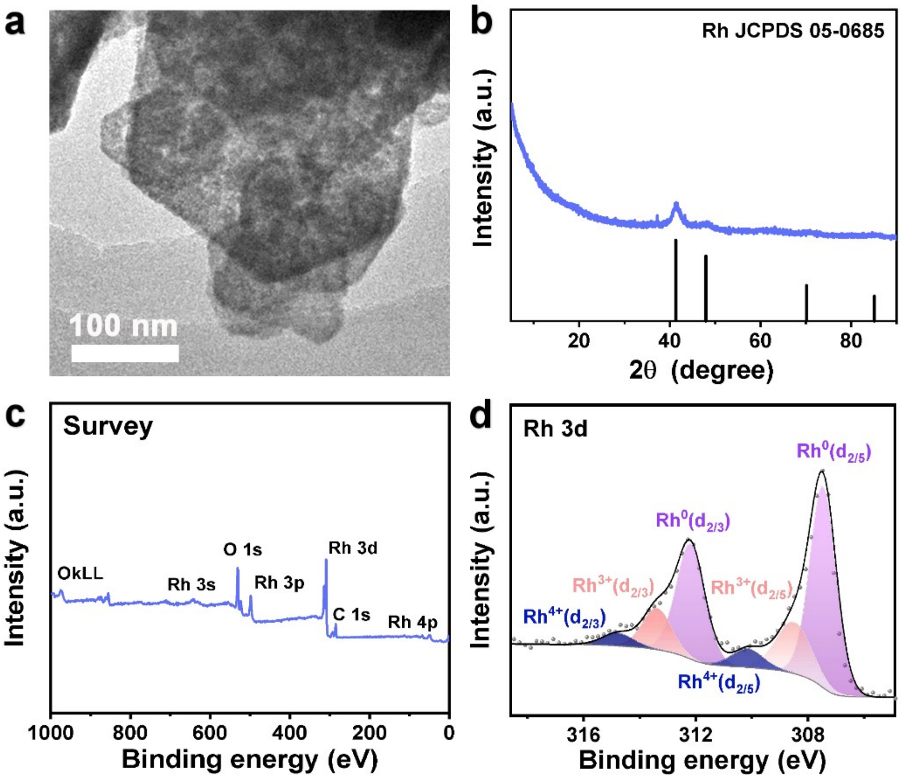

Figure S16. (a) TEM image, (b) XRD pattern, (c) XPS spectra of the survey, and (d) Rh 3d for Rh/RhO_x-500 after 2000 cycles for HzOR in 1.0 M PBS/0.3 M N_2H_4.

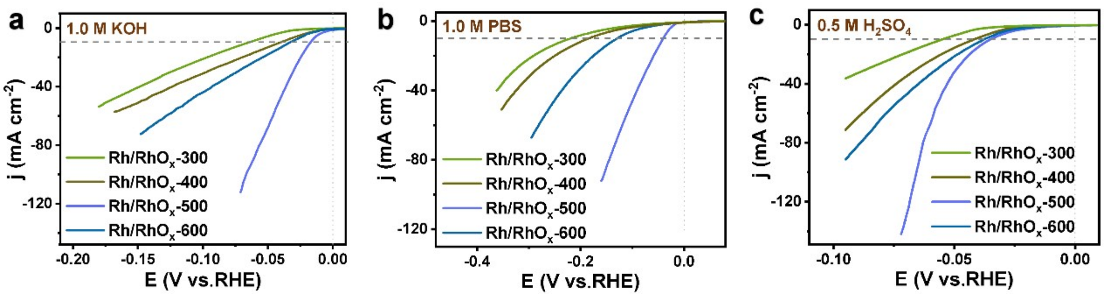

Figure S17. The LSV curves of RhO_x after calcinating at different temperatures for HER in (a) 1.0 M KOH, (b) 1.0 M PBS and (c) 0.5 M H_2SO_4 respectively.

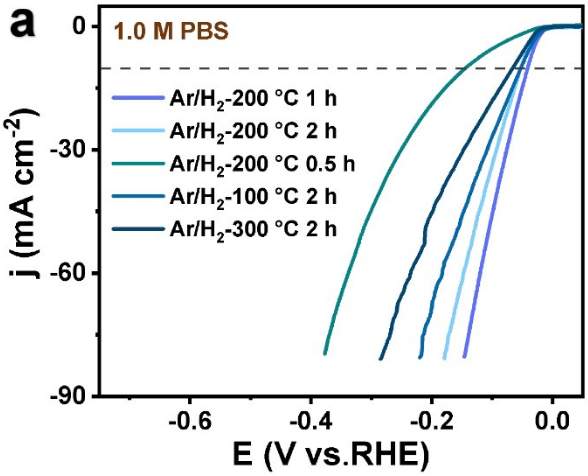

Figure S18. The comparison of performance of Rh/RhO_x-500 obtained at different treatment time and temperature for HER.

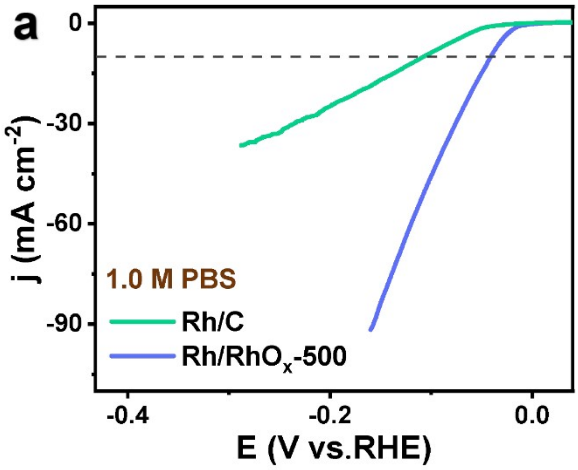

Figure S19. LSV curves of Rh/RhO_x-500 and Rh/C in 1.0 M PBS for HER.

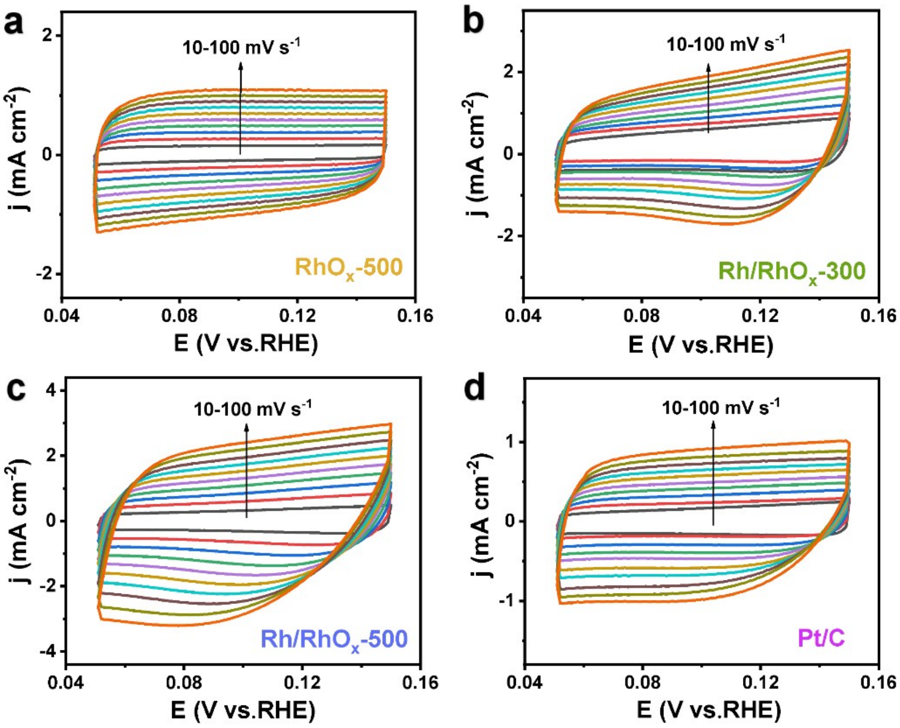

Figure S20. The CV curves of (a) RhO_x-500, b) Rh/RhO_x-300, (c) Rh/RhO_x-500, and (d) Pt/C with the scan rate ranging from 10 to 100 mV s^{-1} in 1.0 M PBS.

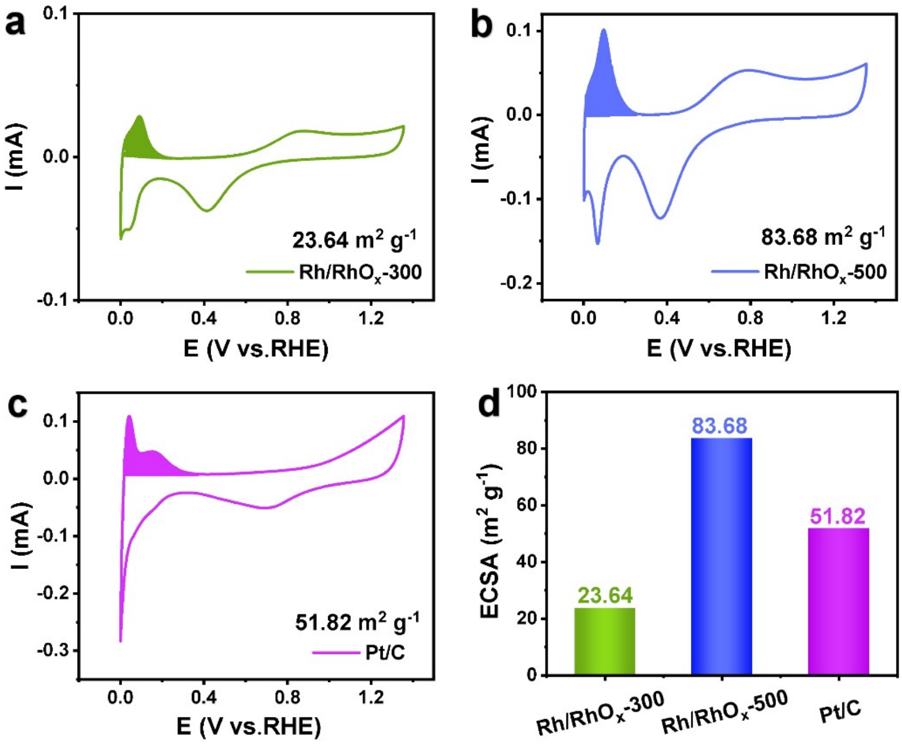

Figure S21. The CV curves of (a) Rh/RhO_x-300, (b) Rh/RhO_x-500, (c) Pt/C in 0.5 M H_2SO_4 solution at a scan rate of 50 mV s^{-1}; (d) The comparison of ECSA values.

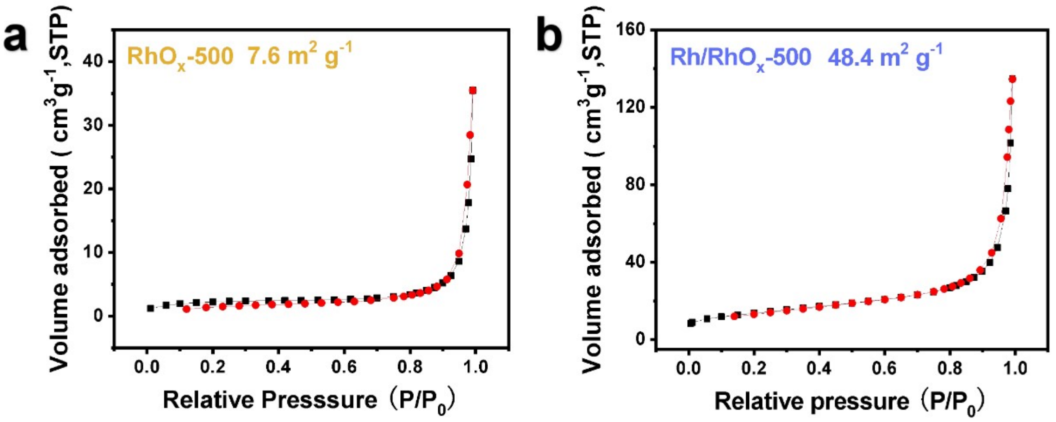

Figure S22. N_2 adsorption-desorption isotherms for (a) RhO$_x$-500, and (b) Rh/RhO$_x$-500.

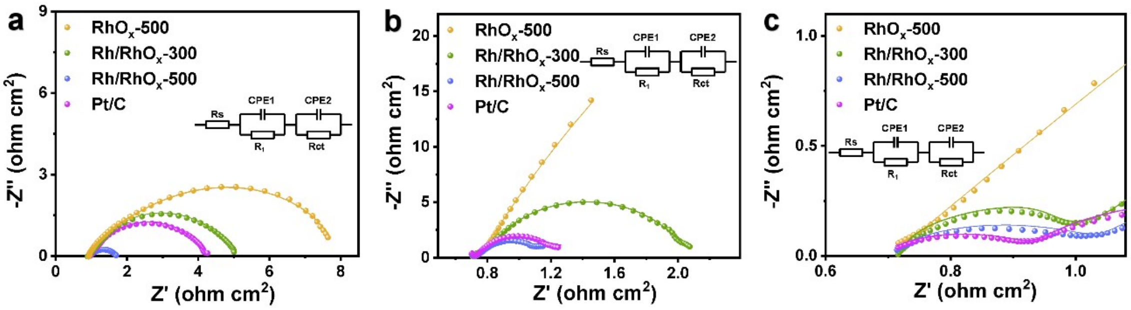

Figure S23. Nyquist plots of different catalysts at -0.03, -0.05 and -0.045V (vs. RHE) in (a) 1.0 M KOH, (b) 1.0 M PBS and (c) 0.5 M H_2SO_4 respectively. The inset is the equivalent circuit model.

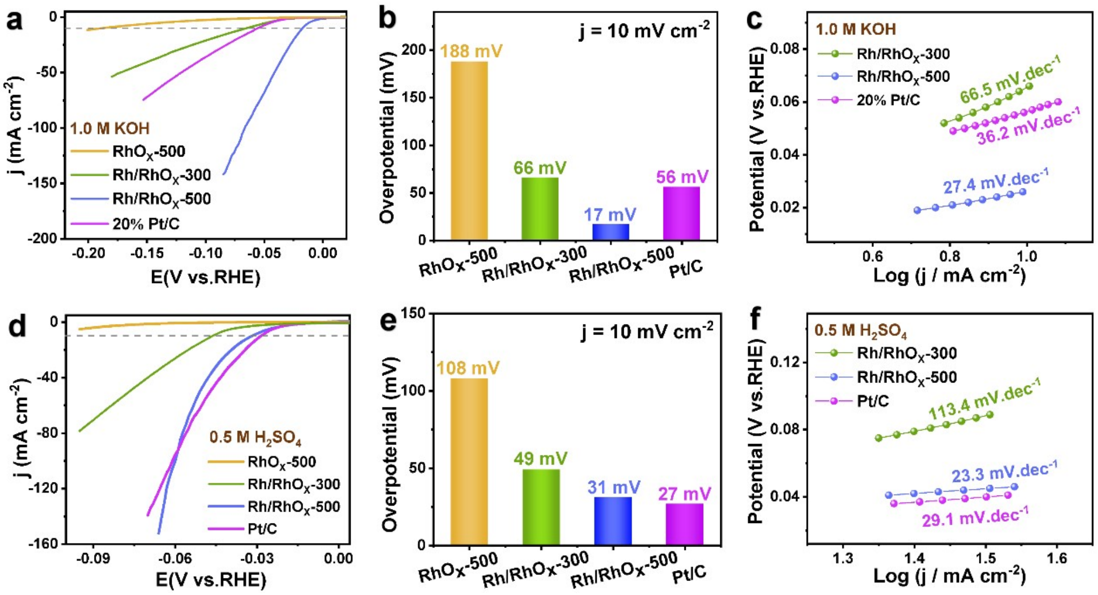

Figure S24. The electrocatalytic activity for HER in alkaline and acid medium. (a) The LSV curves of different catalysts and (b) corresponding overpotential (@10 mA cm^{-2}) comparison in 1 M KOH. (c) Tafel plots derived from (a). (d) The LSV curves of different catalysts and (e) corresponding overpotential (@10 mA cm^{-2}) comparison in 0.5 M H_2SO_4. (c) Tafel plots derived from (d).

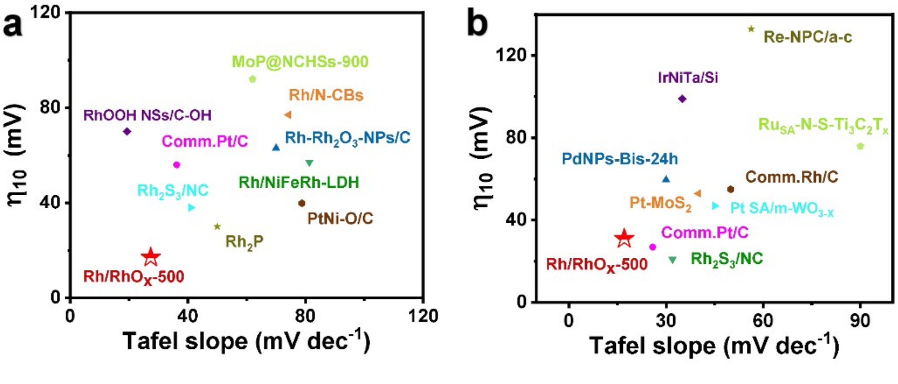

Figure S25. Comparison of overpotential (@ 10 mA cm^{-2}) and Tafel slope for various state-of-the-art HER catalysts in 1.0 M KOH and 0.5 M H_2SO_4, respectively.

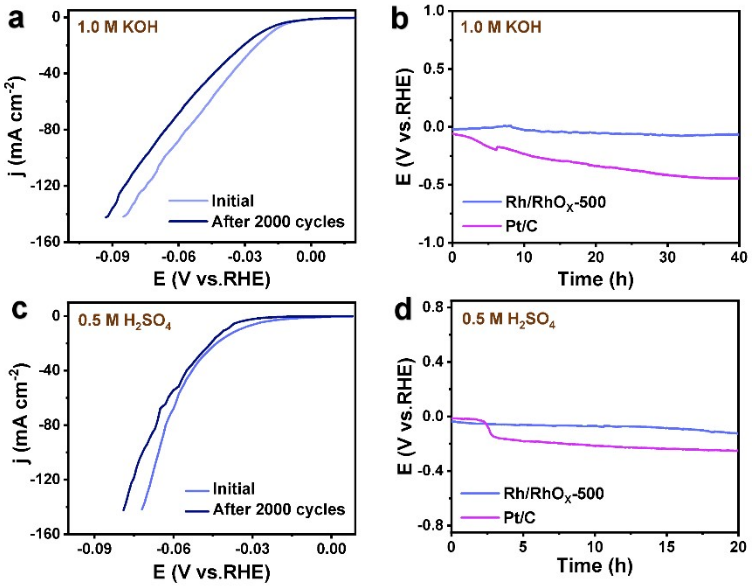

Figure S26. (a) The LSV curves of Rh/RhO$_x$-500 before and after 2000 CV circles, and (b) the chronopotentiometric stability of Rh/RhO$_x$-500 recorded at 10 mA cm^{-2} current density in 1.0 M KOH. (c) The LSV curves of Rh/RhO$_x$-500 before and after 2000 CV circles and (d) the chronopotentiometric stability of Rh/RhO$_x$-500 recorded at 10 mA cm^{-2} current density in 0.5 M H$_2$SO$_4$.

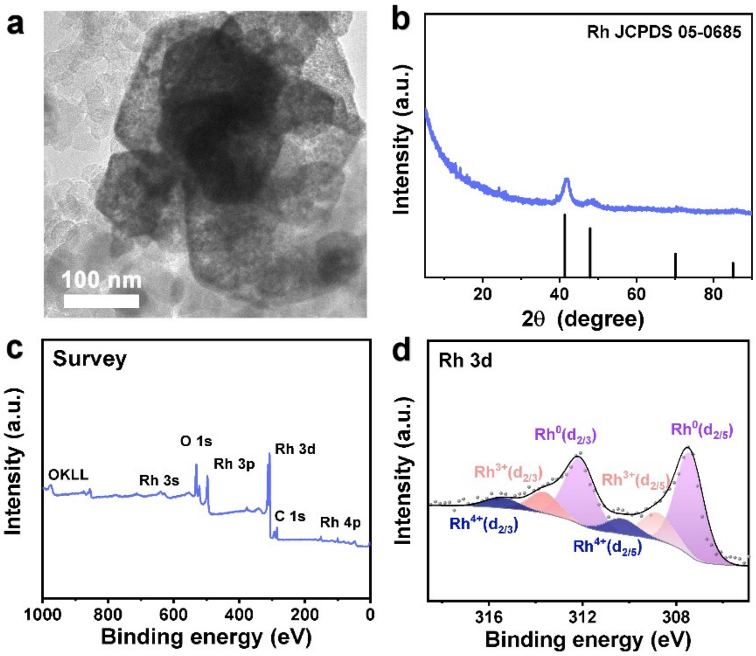

Figure S27. (a) TEM image, (b) XRD pattern, (c) XPS spectra of survey, and (d) Rh 3d for Rh/RhO$_x$-500 after 2000 cycles for HER in 1.0 M PBS .

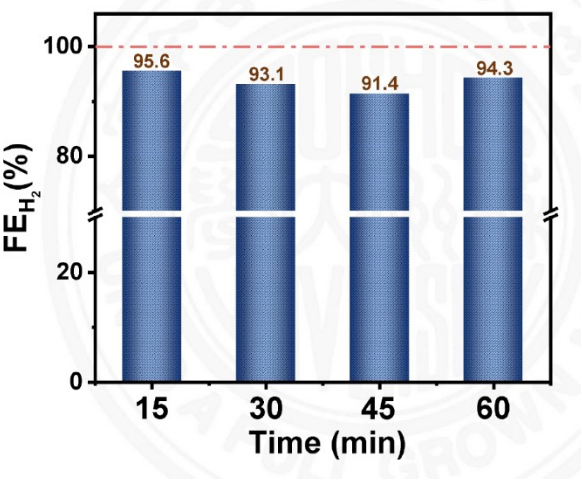

Figure S28. FE_{H2} of OHzS for Rh/RhO_x-500.

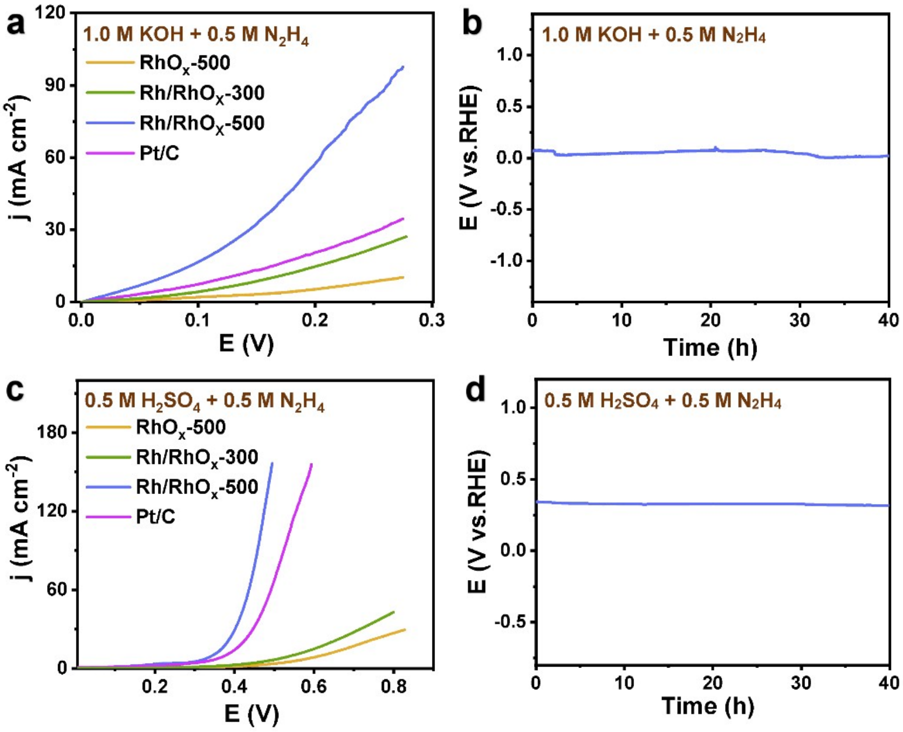

Figure S29. (a) The LSV curves for OHzS in 1.0 M KOH/0.5 M N_2H_4 for different catalysts. (b) The chronoamperometry curve for OHzS recorded at 10 mA cm^{-2} current density in 1.0 M KOH/0.5 M N_2H_4. (c) The LSV curves for OHzS in 0.5 M H_2SO_4/0.5 M N_2H_4 for different catalysts. (d) The chronoamperometry curve for OHzS recorded at 10 mA cm^{-2} current density in 0.5 M H_2SO_4/0.5 M N_2H_4.

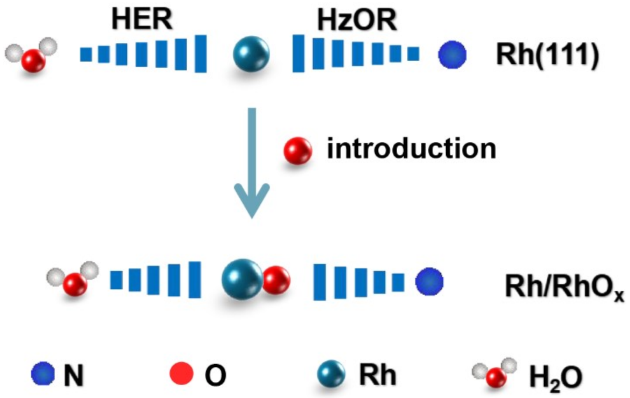

Figure S30. Schematic diagram of the change of bond length due to the introduction of O in HzOR and HER.

Table S1. Comparison of HzOR performances with recently reported catalysts.

Catalysts	Electrolyte	η_{10} (mV)	Tafel slope (mV·dec^{-1})	Reference
Rh/RhO$_x$-500	**1.0 M KOH + 0.5 M N_2H_4**	**-28**	**33.2**	**This work**
	1.0 M PBS + 0.3 M N_2H_4	**94**	**63.6**	
	0.5 M H_2SO_4 + 0.5 M N_2H_4	**247**	**96.2**	
Rh_2S_3/NC	1.0 M KOH + 0.1 M N_2H_4	95	46	8
	1.0 M PBS + 0.1 M N_2H_4	337	196	
	0.5 M H_2SO_4 + 0.1 M N_2H_4	333	91	
RuP_2-CPM	1.0 M KOH + 0.3 M N_2H_4	-70	47.6	9
Cu_1Ni_2-N	1.0 M KOH + 0.5 M N_2H_4	0.5	44.1	10
Ni(Cu)@NiFeP/NM	1.0 M KOH + 0.5 M N_2H_4	6	48.1	11
Ni-NSA	3.0 M KOH + 1.0 M N_2H_4	-8	N/A	12
Co_3Ta/C	3.0 M KOH + 0.5 M N_2H_4	-18	56.9	13
$CoSe_2$	1.0 M KOH + 0.5 M N_2H_4	-17	N/A	14
Rh/N-CBs	1.0 M KOH + 0.5 M N_2H_4	149	38.3	15
Ni_2S_2	1.0 M KOH + 0.2 M N_2H_4	415@100 mA cm^{-2}	95.4	16
D-MoP/rGO	1.0 M KOH + 0.5M N_2H_4	87	N/A	17
Pd-NWNWs	1.0 M KOH + 0.1 M N_2H_4	154@100 mA cm^{-2}	N/A	18
	0.1 M $HClO_4$ + 0.1 M N_2H_4	350@100 mA cm^{-2}	N/A	
Rh_2P uNSs	0.5 M H_2SO_4 + 50 mM N_2H_4	300	N/A	19
Pt (111)	0.1 M $HClO_4$ + 0.001 M NaCl + 0.01 M N_2H_4	450@100 mA cm^{-2}	N/A	20
B-Pd@Rh-NCs	0.1 M KOH + 0.1 M N_2H_4	-31@Onset potential	N/A	S21
	0.1 M $HClO_4$ + 0.1 M N_2H_4	-0.98@Onset potential	N/A	

Table S2. Comparison of HER activities with recently reported catalysts in 1.0 M PBS.

Solution	Catalysts	η_{10} (mV)	Tafel slope (mV·dec^{-1})	Reference
1.0 M PBS	**Rh/RhO$_x$-500**	**39**	**35.9**	**This work**
	Pt/C	47	44.2	This work
	Ni/WC@NC	73	80.9	22
	Li$_x$NiO/Ni	50	66	23
	PdP$_2$@CB	84.6	72.3	24
	CoP/Co-MOF	49	63	25
	RuP$_2$@NPC	57	87	26
	CoP@BCN	122	59	27
	Rh$_2$S$_3$/NC	46	37	8
	S-MoP NPL	142	98	28
	Re-NPC/a-c	164	69.6	29
	FePNPs@NPC	386	136	30
	Fe-CoS$_2$	49	40	31
	Li-IrSe$_2$	120	N/A	32
	NFP/C-3	117	70	33

Table S3. Comparison of HER activities with recently reported catalysts in 1.0 M KOH.

Solution	Catalysts	η_{10} (mV)	Tafel slope (mV·dec^{-1})	Reference
1.0 M KOH	**Rh/RhO$_x$-500**	**17**	**27.4**	**This work**
	Pt/C	56	36.2	This work
	Rh-Rh$_2$O$_3$-NPs/C	63	70.0	34
	Rh/NiFeRh-LDH	57	81.3	35
	RhOOH NSs/C-OH	70	19.3	36
	Rh-doped CoFe-LDH	28	42.8	37
	Rh/N-CBs	77	74.2	15
	Rh$_2$S$_3$/NC	38	41.0	8
	PtNi-O/C	39.8	78.8	38
	Rh$_2$P	30	50	39
	Ru@CN	32	53	40
	Pt-WS$_2$	36	65	41
	MoP@NCHSs-900	92	62	42
	Cu$_1$Ni$_2$-N	71.4	106.5	10
	Co$_2$P@CP	67.5	59.7	43
	RuP$_2$-CPM	24	47.6	9

Tabel S4. Comparison of HER activities with recently reported catalysts in 0.5 M H_2SO_4.

Solution	Catalysts	η_{10} (mV)	Tafel slope ($mV\cdot dec^{-1}$)	Reference
0.5 M H_2SO_4	**Rh/RhO_x-500**	**31**	**23.3**	**This work**
	Pt/C	27	29.1	This work
	Comm.Rh/C	55	50	34
	Rh_2S_3/NC	21	32	8
	Ru_A-N-S-$Ti_3C_2T_x$	76	90	44
	Pt-MoS_2	53	40	45
	RuP_2@NPC	38	38	26
	Pt SA/m-WO_{3-x}	47	48	46
	Pt-Ru dimer	50	28.9	47
	Pt NWs/SL-$Ni(OH)_2$	95	N/A	48
	IrNiTa/Si	99	35	49
	Pd NPs-Bis-24h	59.6	30	50
	Re-NPC/a-c	133	56.3	29
	W-CoP NAs/CC	89	58	51
	S-MoP NPL	86	34	28

Tabel S5. Comparison of OHzS performances with recently reported catalysts.

Catalysts	Electrolyte	Cell Voltage (V) j = 10 mA cm^{-2}	Reference
Rh/RhO$_x$-500	**1.0 M KOH + 0.5 M N_2H_4**	**0.068** **0.279@100 mA cm^{-2}**	**This work**
	1.0 M PBS + 0.3 M N_2H_4	**0.268**	
	0.5 M H_2SO_4 + 0.5 M N_2H_4	**0.348**	
Rh_2S_3/NC	1.0 M KOH + 0.1 M N_2H_4	0.108	8
	1.0 M PBS + 0.1 M N_2H_4	0.286	
	0.5 M H_2SO_4 + 0.1 M N_2H_4	0.375	
Cu_1Ni_2-N	1.0 M KOH + 0.5 M N_2H_4	0.24	10
Ni(Cu)@NiFeP/NM	1.0 M KOH + 0.5 M N_2H_4	0.491@100 mA cm^{-2}	11
$CoSe_2$	1.0 M KOH + 0.5 M N_2H_4	0.164	14
Ni_3N-Co_3N	1.0 M KOH + 0.1 M N_2H_4	0.071	52
Ni_2P	1.0 M KOH + 0.5 M N_2H_4	0.45@100 mA cm^{-2}	53
Ni_3S_2	1.0 M KOH + 0.2 M N_2H_4	0.867@100 mA cm^{-2}	16
Ni(Cu)alloy	1.0 M KOH + 0.5 M N_2H_4	0.41@100 mA cm^{-2}	54
Au@Rh ultra-NWs	1.0 M KOH + 0.1 M N_2H_4	0.18	55
CoS_2/TiM	1.0 M KOH + 0.1 M N_2H_4	0.81@100 mA cm^{-2}	56
CoP/NCNT-CP	1.0 M KOH + 0.5 M N_2H_4	0.89	57
Rh/N-CBs	1.0 M KOH + 0.5M N_2H_4	0.2@20 mA cm^{-2}	15

Table S6. Gibbs free energy changes of reaction intermediates on hydrazine reduction reaction.

HzOR	**(NH_2NH_2)**	***NH_2NH_2**	***$NHNH_2$**	***NHNH**	***NNH**	***vN_2**	**(N_2)**
Rh(111)	0.00	-0.97	-0.73	-0.56	-0.53	-1.29	-0.87
Rh/RhO_x	0.00	-0.95	-0.84	-0.66	-0.50	-1.34	-0.87

Table S7. The reaction energy barrier for H_2O dissociation.

HER (neb)	**Initial ($2H_2O$)**	**TS**	**Final (HOHOH + $1/2H_2$)**
Pt(111)	0	0.721 eV	-0.433 eV
Rh(111)	0	0.466 eV	-0.198 eV
Rh(111)-Rh-O	0	0.419 eV	-0.192 eV
Pt(111)	0	0.721 eV	-0.433 eV

References

1. G. Kresse, J. Hafner, *Phys. Rev. B*, 1993, **47**, 558-561.
2. G. Kresse, J. Furthmüller, *Comput. Mater. Sci.*, 1996, **6**, 15-50.
3. G. Kresse, J. Furthmüller, *Phys. Rev. B*, 1996, **54**, 11169-11186.
4. J. P. Perdew, K. Burke and M. Ernzerhof, *Phys. Rev. Lett.*, 1996, **77**, 3865-3868.
5. S. Grimme, J. Antony, S. Ehrlich and H. Krieg, *J. Chem. Phys.*, 2010, **132**, 154104.
6. P. E. Blöchl, *Phys. Rev. B*, 1994, **50**, 17953-17979.
7. G. Kresse, D. Joubert, *Phys. Rev. B*, 1999, **59**, 1758-1775.
8. C. X. Zhang, H. X. Liu, Y. F. Liu, X. J. Liu, Y. Y. Mi, R. J. Guo, J. Q. Sun, H. H. Bao, J. He, Y. Qiu, J. Q. Ren, X. J. Yang, J. Luo and G. Z. Hu, *Small Methods*, 2020, **4**, 2000208.
9. Y. P. Li, J. H. Zhang, Y. Liu, Q. Z. Qian, Z. Y. Li, Y. Zhu, G. Q. Zhang, *Sci. Adv.*, 2020, **6**, eabb4197.
10. Z. Y. Wang, L. Xu, F. Z. Huang, L. B. Qu, J. T. Li, K. A. Owusu, Z. I. Liu, Z. F. Lin, B. H. Xiang, X. Liu, K. K. Zhao, X. B. Liao, W. Yang, Y. B. Cheng, L. Q. Mai, *Adv. Energy Mater.*, 2019, **9**, 1900390.
11. Q. Q. Sun, M. Zhou, Y. Q. Shen, L. Y. Wang, Y. Ma, Y. B. Li, X. Bo, Z. L. Wang, C. Zhao, *Catal.*, 2019, **373**, 180-189.
12. Y. Kuang, G. Feng, P. S. Li, Y. M. Bi, Y. P. Li and X. M. Sun, *Angew. Chem. Int. Ed.*, 2016, **55**, 693-697.
13. G. Feng, L. An, B. Li, Y. X. Zuo, J. Song, F. H. Ning, N. Jiang, X. P. Cheng, Y. F. Zhang and D. G. Xia, *Nat. Commun.*, 2019, **10**, 4514.
14. J. Y. Zhang, H. M. Wang, Y. F. Tian, Y. Yan, Q. Xue, T. He, H. F .Liu, C. D. Wang, Y. Chen and B. Y. Xia, *Angew. Chem. Int. Ed.*, 2018, **57**, 7649-7653.
15. N. Jia, Y. P. Liu, L. Wang, P. Chen, X. B. Chen, Z. W. An and Y. Chen, *ACS Appl. Mater. Interfaces*, 2019, **11**, 35039-35049.

16. G. Q. Liu, Z. T. Sun, X. Zhang, H. J. Wang, G. Z. Wang, X. J. Wu, H. Zhang and H. J. Zhao, *J. Mater. Chem. A*, 2018, **6**, 19201-19209.

17. Y. Gao, Q. Wang, T. He, J. Y. Zhang, H. Sun, B. Zhao, B. Y. Xia, Y. Yan and Y. Chen, *Inorg. Chem. Front.*, 2019, **6**, 2686-2695.

18. F. M. Li, Y. G. Ji, S. M. Wang, S. N. Li and Y. Chen, *Electrochim. Acta*, 2015, **176**, 125-129.

19. Y. Zhao, N. Jia, X. R. Wu, F. M. Li, P. Chen, P. J. Jin, S. W. Yin and Y. Chen, *Appl. Catal. B,* 2020, **270**, 118880.

20. R. Gisbert, A. Boronat-González, J. M. Feliu and E. Herrero, *ChemElectroChem*, 2017, **4**, 1130-1134.

21. G. J. Wang, S. C. Jing and Y. W. Tan, *Sci. Rep.*, 2017, **7**, 16465.

22. Y. Y. Ma, Z. L. Lang, L. K. Yan, Y. H. Wang, H. Q. Tan, K. Feng, Y. J. Xia, J. Zhong, Y. Liu, Z. H. Kang and Y. G. Li, *Energy Environ. Sci.*, 2018,**11**, 2114-2123.

23. K. Lu, Y. Z. Liu, F. Lin, I. A. Cordova, Y. Cheng, S. Y. Gao, B. M. Li, B. Peng, H. P. Xu, J. Kaelin, D. Coliz, C. Wang, Y. Y. Shao and Y. W. Cheng, *J. Am. Chem. Soc.*, 2020, **142**, 12613-12619.

24. F. Luo, Q. Zhang, X. X. Yu, S. L. Xiao, Y. Ling, H. Hu, L. Guo, Z. H. Yang, L. Huang, W. W. Cai and H. S. Cheng, *Angew. Chem.*, 2018, **130**, 15078-15083.

25. T. Liu, P. Li, N. Yao, G. Z. Cheng, S. L.Chen, W. Luo and Y. D. Yin, *Angew. Chem. Int. Ed.*, 2019, **58**, 4679-4684.

26. Z. H. Pu, I. S. Amiinu, Z. Kou, W. Q. Li and S. C. Mu, *Angew. Chem.*, 2017, **129**, 11717-11722.

27. H. Tabassum, W. H. Guo, W. Meng, A. Mahmood, R. Zhao, Q. F. Wang and R. Q. Zou, Adv. *Energy Mater.*, 2017, **7**, 1601671.

28. K. Liang, S. Pakhira, Z. Z. Yang, A. Nijamudheen, L. C. Ju, M. Y. Wang, C. I. Aguirre-Velez, G. E. Sterbinsky, Y. G. Du, Z. X. Feng, J. L. Mendoza-Cortes and Y. Yang, *ACS Catal.*, 2019, **9**, 651-659.

29. M. J. Kim, Z. J. Yang, J. H. Park, S. M. Yoon and B. A. Grzybowski, *ACS Appl. Nano Mater.*, 2019, **2**, 2725-2733.

30. Z. H. Pu, I. S. Amiinu, C. T. Zhang, W. Min, Z. K. Kou and S. C. Mu, *Nanoscale*, 2017, **9**, 3555-3560.

31. X. J. Liu, J. He, S. Z Zhao, Y. P. Liu, Z. Zhao, J. Luo, G. Z. Hu, X. M Sun and Y. Ding, *Nat. Commun.*, 2018, **9**, 4365.

32. T. T. Zheng, C. Y. Shang, Z. H. He, X. Y. Wang, C. Cao, H. L. Li, R. Si, B. C. Pan, S. M. Zhou and J. Zeng, *Angew. Chem. Int. Ed.*, 2019, **58**, 14764-14769.

33. X. F. Lu, L. Yu and X. W. Lou, *Sci. Adv.*, 2019, **5**, eaav6009.

34. M. K. Kundu, R. Mishra, T. Bhowmik and S. Barman, *J. Mater. Chem. A*, 2018, **6**, 23531-23541.

35. B. W. Zhang, C. Q. Zhu, Z. S. Wu, E. Stavitski, Y. H. Lui, T. H. Kim, H. Liu, L. Huang, X. C. Luan, L. Zhou, K. Jiang, W. Y. Huang, S. Hu, H. L. Wang and J. S. Francisco, *Nano Lett.*, 2020, **20**, 136-144.

36. S. X. Bai, M. Xie, T. Cheng, K. L. Cao, Y. Xu and X. Q. Huang, *Nano Energy*, 2020, **78**, 105224.

37. K. Y. Zhu, J. Y. Chen, W. J. Wang, J. W. Liao, J. C. Dong, M. O. L. Chee, N. Wang, P. Dong, P. M. Ajayan, S. Gao, J. F. Shen and M. X. Ye, *Adv. Funct. Mater.*, 2020, **30**, 2003556.

38. Z. P. Zhao, H. T. Liu, W. P. Gao, W. Xue, Z. Y. Liu, J. Huang, X. Q. Pan and Y. Huang, *J. Am. Chem. Soc.*, 2018, **140**, 9046-9050.

39. F. L. Yang, Y. M. Zhao, Y. S. Du, Y. T. Chen, G. Z. Cheng, S. L. Chen and W. Luo, *Adv. Energy Mater.*, 2018, **8**, 1703489.

40. J. Wang, Z. Z. Wei, S. J. Mao, H. R. Li and Y. Wang, *Energy Environ. Sci.*, 2018, **11**, 800-8062018.

41. K. Tang, X. F. Wang, Q. Li and C. L. Yan, *Adv. Mater.*, 2018, **30**, 1704779.

42. Q. Q. Hou, Y. Wu, S. Zhou, Y. Y. Wei, J. Caro and H. H. Wang, *Angew. Chem. Int. Ed.*, 2019, **58**, 2.

43. Y. Zhang, L. Gao, E. J. M. Hensen and J. P. Hofmann, *ACS Energy Lett.*, 2018, **3**, 1360-1365.

44. V. Ramalingam, P. Varadhan, H. C. Fu, H. Kim, D. L. Zhang, S. M. Chen, L. Song, D. Ma, Y. Wang, H. N. Alshareef and J. H. He, *Adv. Mater.*, 2019, **31**, 1903841.

45. X. Huang, Z. Y. Zeng, S. Y. Bao, M. F. Wang, X. Y. Qi, Z. X. Fan and H. Zhang, *Nat. Commun.*, 2013, **4**, 1444.

46. J. Park, S. Lee, H. E. Kim, A. Cho, S. Kim, Y. J. Ye, J. W. Han, H. Lee, J. H. Jang and J. Lee, *Angew. Chem.*, 2019, **131**,16184-16188.

47. L. Zhang, R. T. Si, H. S. Liu, N. Chen, Q. Wang, K. Adair, Z. Q. Wang, J. T. Chen, Z. X. Song, J. J. Li, M. N. Banis, R. Y. Li, T. K. Sham, M. Gu, L. M. Liu, G. A. Botton and X. L. Sun, *Nat. Commun*., 2019, **10**, 4936.

48. H. J. Yin, S. L. Zhao, K. Zhao, A. Muqsit, H. J. Tang, L. Chang, H. J. Zhao, Y. Gao and Z. Y. Tang, *Nat. Commun.*, 2015, **6**, 6430.

49. Z. J. Wang, M. X. Li, J. H Yu, X. B. Ge, Y. H. Liu and W. H. Wang, *Adv. Mater.*, 2020, **32**, 1906384.

50. H. F. Cheng, N. L.Yang, G. G. Liu, Y. Y. Ge, J. T. Huang, Q. B. Yun, Y. H. Du, C. J. Sun, B. Chen, J. W. Liu and H. Zhang, *Adv. Mater.*, 2020, **32**, 1902964.

51. X. Q. Wang, Y. F. Chen, B. Yu, Z. G. Wang, H. Q. Wang, B. C. Sun. W. X. Li, D. X. Yang and W. L. Zhang, *Small*, 2019, **15**, 1902613.

52. Q. Z. Qian, J. H. Zhang, J. M. Li, Y. P. Li, X. Jin, Y. Zhu, Y. Liu, Z. Li, A. E. Harairy, C. Xiao, G. Q. Zhang and Y. Xie, *Angew. Chem. Int. Ed.*, 2021, **60**, 5984-5993.

53. C. Tang, R. Zhang, W. B. Lu, Z. Wang, D. N. Liu, S. Hao, G. Du, A. M. Asiri and X. Sun, *Angew. Chem.*, 2017, **129**, 860.

54. Q. Q. Sun, L. Y. Wang, Y. Q. Shen, M. Zhou, Y. Ma, Z. L. Wang and C. Zhao, *ACS Sustain. Chem. Eng.*, 2018, **6**, 12746-12754.

55. Q. Xue, H. Huang, J. Y. Zhu, Y. Zhao, F. M. Li, P. Chen and Y. *Chen, Appl. Catal.*, *B* 2020, **278**, 119269.

56. X. Ma, J. M. Wang, D. N. Liu, R. M. Kong, S. Hao, G. Du, A. M. Asiri and X. P. Sun, *New J. Chem.*, 2017, **41**, 4754-4757.

57. L. Wang, J. H. Cao, X. D. Cheng, C. J. Lei, Q. Z. Dai, B. Yang, Z. J. Li, M. A. Younis, L. C. Lei, Y. Hou and K. K. Ostrikov, *ACS Sustainable Chem. Eng.*, 2019, **7**, 10044-10051.